Journal of Hazardous Materials 205–206 (2012) 17–23

Contents lists available at SciVerse ScienceDirect

Journal of Hazardous Materials

journal homepage: www.elsevier.com/locate/jhazmat

Nano-magnetic particles as multifunctional microreactor for deep desulfurization

Xinai Cui [a], Dongdong Yao [a], Hong Li [b], Juxiang Yang [c], Daodao Hu [a,*]

[a] Engineering Research Center of Historical and Cultural Heritage Protection, Ministry of Education, School of Materials Science and Engineering, Shaanxi Normal University, Xi'an 710062, China
[b] College of Environment and Chemical Engineering, Xi'an Polytechnic University, Xi'an 710048, China
[c] Department of Chemistry, Xi'an University of Arts and Science, Xi'an 710065, China

ARTICLE INFO

Article history:
Received 13 May 2011
Received in revised form
10 November 2011
Accepted 18 November 2011
Available online 29 November 2011

Keywords:
Deep desulfurization
Amphiphilic composite material
Magnetic nanoparticles
Diphase catalysis

ABSTRACT

Oxidation of dibenzothiophene with hydrogen peroxide using a recyclable amphiphilic catalyst has been studied. The catalyst was synthesized by surfacely covering magnetic silica nanospheres (MSN) with the complexes between 3-(trimethoxysilyl)-propyldimethyloctadecyl ammonium chloride (AEM) and phosphotungstic acid (PTA). The morphology and components of the composite material were characterized by TEM, EDX, XPS, FT-IR, and VSM, respectively. The effects of several factors on desulfurization reactivity were systematically investigated. The results showed that the composite nanospheres have core/shell structure with the properties of amphiphilicity and superparamagnetism. The composite nanospheres have high catalytic activity in the oxidation of dibenzothiophene to corresponding sulfones by hydrogen peroxide under mild reaction conditions. The sulfur level could be lowered from 487 ppm to less than 0.8 ppm under optimal conditions. Additionally, the amphiphilic catalyst and the oxidized product could be simultaneously separated from medium by external magnetism, and the recovered composite material could be recycled for three times with almost constant activity.

1. Introduction

Sulfur oxide produced by the combustion of sulfur-containing organic compounds in fuel oils is one of the major air pollutants. To protect the environment, some stringent environmental regulations about the discharges of sulfur oxide have been enacted [1,2]. To eliminate undesirable sulfur-containing compounds or to convert them into innocuous forms, various alternative processes, which differed from the hydrodesulfurization [3,4], have been employed. Generally, the processes include adsorption [5,6], extraction [7], oxidation [8–11] and bioprocesses [12,13]. The need for sustainable chemistry and clean technologies has stimulated the research for new, environmentally friendly desulfurization systems. Li et al. [14] applied a recoverable catalyst assembled in emulsion to catalytic-oxidation ultra-deep desulfurization. The catalyst, $[(C_{18}H_{37})_2N^+(CH_3)_2]_3[PW_{12}O_{40}]$, demonstrated high performance, lowering the sulfur level from approximately 500 ppm to 0.1 ppm without changing the properties of the diesel. Furthermore, the catalyst was separated from the diesel by demulsification. The product in the diesel was removed by a polar extractant. The report shows that selective catalytic oxidation combined with extraction is one of the most promising methods of ultra-deep desulfurization. Additionally, the W/O emulsion structure with water pool and surfactant shell is efficient to enhance the diphase catalysis. However, the method has a relatively complex process and the emulsion structure is not stable because it formed only via supramolecular interaction which is easily affected by the subtle change of environment factors and the concentration of surfactant.

Recently, we had reported a novel methodology for creating insoluble catalysts with hydrogel core and amphiphilic phase transfer catalyst–shell structure similar to W/O emulsion droplet [15,16]. The results indicated that the prepared catalysts not only were valuable for deep oxidation desulfurization but also can extract the polar product from system. Compared with the recoverable catalyst assembled in emulsion, this protocol makes desulfurization process simple. However, the catalytic efficiency was unsatisfied due to the supporting particles with bigger size. Therefore, to prepare an easy-separated phase transfer catalyst with smaller size is valuable to enhance catalytic efficiency.

In view of the fact that paramagnetic nano-particles are easily separated under external magnetic field, we proposed immobilization of alkyl quaternary ammonium surfactant/Keggin-type polyoxometalate complexes on nanomagnetic silica as a nanoreactor to improve our original method. The results indicated that the catalytic efficiency of the prepared nanomagnetic particles in deep oxidation desulfurization was obviously higher than that of

* Corresponding author. Tel.: +86 29 81530700.
E-mail address: daodaohu@snnu.edu.cn (D. Hu).

0304-3894/$ – see front matter © 2011 Elsevier B.V. All rights reserved.
doi:10.1016/j.jhazmat.2011.11.063

our original report. Desulfurization rate was increased from 45% in original system to above 90% in present one [15]. The turn over frequency (TOF) was about 0.5147 min^{-1}, which is higher than that of the emulsion system mentioned above [14]. For the improved system, the catalyst and oxidized product can be simultaneously separated from medium under external magnetic field, and the recovered catalyst could be recycled for three times with almost constant activity. This research not only provides an efficient method to desulfurize from organic medium but also develops a new catalytic material used in oil/water diphase organic chemistry.

2. Experimental

2.1. Materials

All chemicals were analytical grade and used without further purification. Water used in the experiments was double-distilled.

2.2. Preparation of magnetic silica/AEM–phosphotungstic acid nanospheres (MSN/AEM–PTA)

The corresponding preparation process is shown in Scheme 1. The phase transfer catalytic material with smaller size was simply prepared by anchoring the organosiloxane 3-(trimethoxysilyl)-propyldimethyloctadecyl ammonium chloride (AEM) on the surface of magnetic silica nanospheres (MSN), then exchanging chloride ions with phosphotungstic acid anions.

2.2.1. Preparation of magnetic silica/AEM nanospheres (MSN/AEM)

MSN were synthesized by a water-in-oil microemulsion technique according to the previous report [17]. MSN/AEM were prepared by the condensation reaction between Si–OH groups on the surface of MSN and that derived from hydrolyzed AEM in solution. A typical synthesis is as follows. MSN (0.100 g) were immersed in 500 μL anhydrous methanol containing a given amount of AEM in a laboratory dish. In the experiment, the different amounts of AEM (5%, 10% and 15% (v/v)) were added for consideration of changing the amount of AEM loaded on MSN. After volatilization of solvent, the dish was placed in a closed beaker containing water for 40 min. Then, put it in a preheated oven (60 °C) immediately to make AEM carry out hydrolysis and condensation for 12 h. After the heat-treated samples were washed with anhydrous alcohol, MSN/AEM nanoparticles were obtained.

2.2.2. Preparation of MSN/AEM–phosphotungstic acid nanospheres (MSN/AEM–PTA)

As a quaternary ammonium salt, AEM can react with PTA by ion-exchange reaction [15]. Based on this principle, PTA can be immobilized on MSN/AEM to form MSN/AEM–PTA. The typical procedure is as follows. A vessel containing MSN/AEM (with 1% AEM) suspended in 20 mL saturated PTA ethanol solution was placed in a constant temperature shaking bath at 38 °C for 2 days to ensure complete ion-exchange. After washing by anhydrous alcohol, MSN/AEM–PTA nanoparticles with 1% AEM were finally obtained. Similarly, MSN/AEM–PTA loaded the different amounts of PTA could be obtained by using MSN/AEM with the different amounts of AEM.

2.3. Catalytic test

The typical process is as follows. DBT (0.0625 g) was dissolved in decahydronaphthalene (25 mL) in a round bottom flask equipped with a mechanical stirrer. The suspension, MSN/AEM–PTA (0.12 g) ultrasonically dispersed in the mixture of H_2O_2 solution (0.30 mL, 30 wt%) and decahydronaphthalene (5 mL), was added to the flask under vigorous stirring. During the reaction, the mixture was stirred at 600 rpm under 50 °C. The residue concentration of DBT in decahydronaphthalene was periodically determined by GC analysis. After completion of the reaction, MSN/AEM–PTA nanoparticles were separated from the reaction system under external magnetic field. The separated MSN/AEM–PTA nanoparticles were washed with acetone for reuse, and the eluent was used to characterize the oxidized product (the corresponding sulfone of DBT) by GC analysis. The process was schematically shown in the insertion of Scheme 2.

2.4. Characterization

The morphology of samples was examined by Japanese Electronics Company JEM-2100 Transmission Electron Microscopy (TEM) operating at 200 kV. The elements in the samples were probed by energy-dispersive X-ray (EDX) spectroscopy accessory to the Philips scanning electron microscopy (SEM) and X-ray photoelectron spectrum (XPS) performed on an AXISULTRA (Kratos Analytical Ltd.). Thermogravimetric analyses (TGA) were performed using a SDT Q600 V8.0 Build95 instrument. The composite powders were heated to 750 °C at a heating rate 5 °C/min in oxygen atmosphere. The IR spectra were recorded on an AVTAR360 Nicolet Fourier transform infrared (FT-IR) spectrometer using a KBr pellet. Magnetic characterization of the samples was carried out on a vibrating sample magnetometer (VSM, LakeShore 7307) at room temperature.

The residue concentration of DBT in decahydronaphthalene and the corresponding sulfone of DBT in the eluent were analyzed via Agilent 6820N gas chromatography (equipped with capillary column (19091s-413, 30 m × 0.2 mm, id × 0.5 μm)) coupled with flame ionization detector (Agilent H9261). Analysis conditions were as follows. Injection port temperature, 280 °C; detector temperature, 300 °C; oven temperature program, 80 °C, hold for 0 min, 80–180 °C at a 20 °C/min gradient, hold for 2 min, 180–240 °C at a 20 °C/min gradient, hold for 2 min, 240–280 °C at a 20 °C/min gradient, hold for 2 min; injection volume of sample, 0.2 μL.

3. Results and discussion

3.1. Characterizations of MSN, MSN/AEM and MSN/AEM–PTA

3.1.1. TEM, EDX, TGA and XPS characterizations

These technologies used here are to characterize the spatial distribution of the main components in MSN/AEM–PTA. Fig. 1a showed the TEM image of MSN synthesized by the microemulsion method. MSN had an average diameter of less than 20 nm, and the nanomagnetic particles were densely entrapped within SiO_2 shell. The presence of SiO_2 and magnetic particles also were testified by the FT-IR characterization (see the corresponding section). The nanomagnetic particles dotted in silica can restrain H_2O_2 from decomposing by the exposed iron oxides [18] when the prepared composite material is subsequently used in oxidative desulfurization with H_2O_2. Moreover, the centralization of the magnetic particles in the composite nanoparticles is favorable to enhance the magnetism. Additionally, the surface Si–OH groups can easily react with siloxane coupling agents (AEM) to provide ideal anchorage for subsequent formation of phase-transfer catalysis layer with ordered structure. The TEM images of MSN/AEM and MSN/AEM–PTA with 1% AEM were showed in Fig. 1b and c. The morphology and size of MSN/AEM and MSN/AEM–PTA do not have too much change compared to MSN. In order to get some information on the elemental composition and distribution on the surface of the samples, MSN, MSN/AEM and MSN/AEM–PTA with 5% AEM were characterized by using EDX analysis. The corresponding results were shown in Fig. 2. The amount of Fe determined in

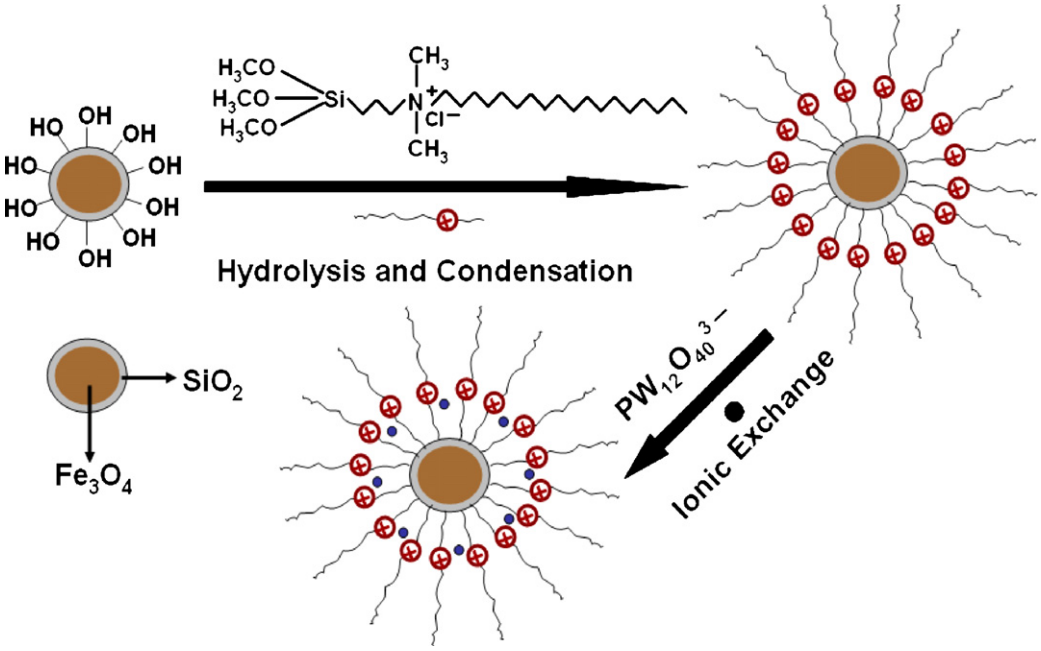

Scheme 1. The process for preparation of MSN/AEM–PTA.

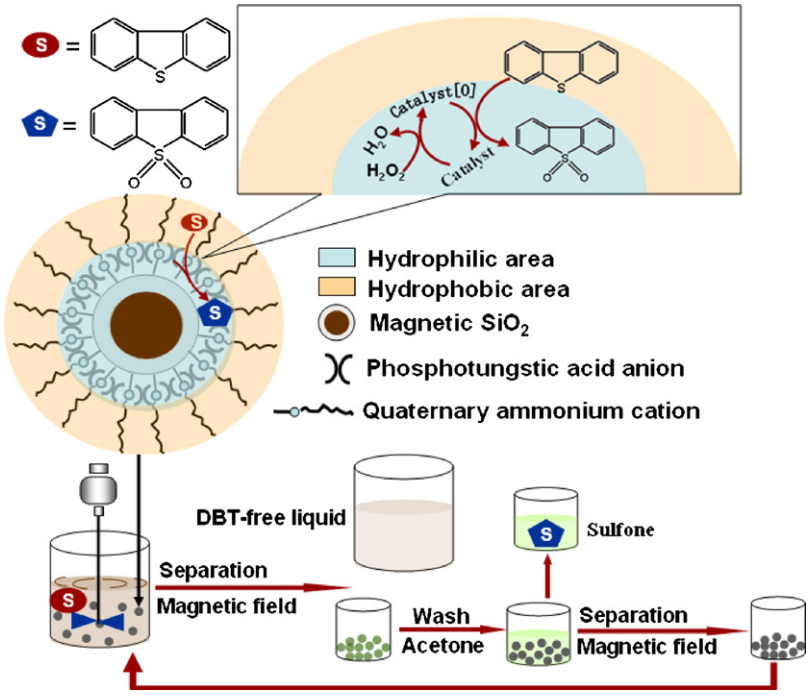

Scheme 2. The oxidation of DBT to sulfone catalyzed by MSN/AEM–PTA particles.

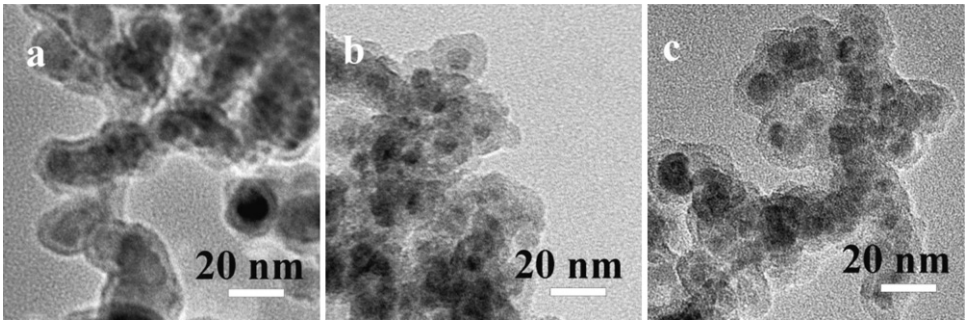

Fig. 1. HR-TEM images of MSN (a), MSN/AEM (b) and MSN/AEM–PTA (c) with 1% AEM.

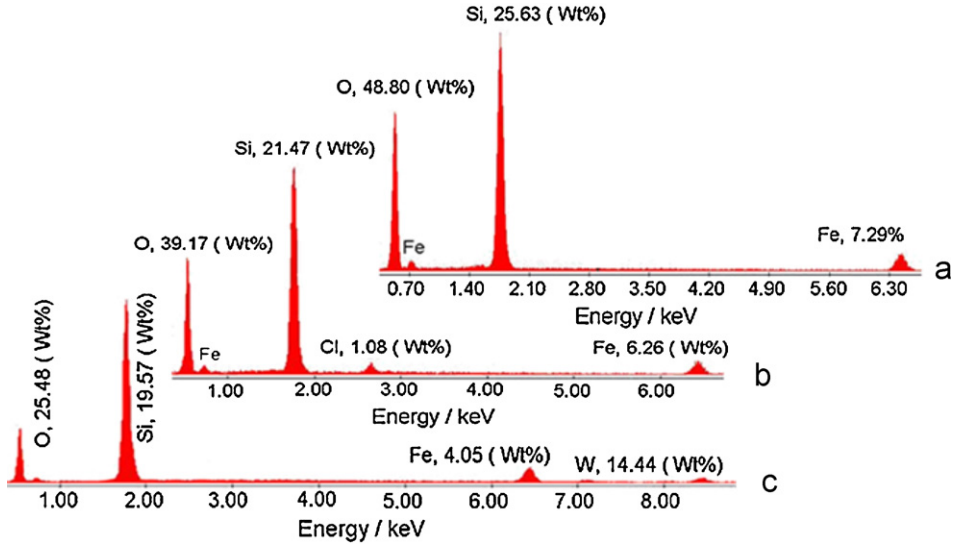

Fig. 2. The EDX spectra of MSN (a), MSN/AEM (b) and MSN/AEM–PTA (c) with 5% AEM.

MSN (7.29 wt%, Fig. 2a) is much lower than that theoretically calculated in Fe_3O_4 (72.4 wt%), indicating that Fe_3O_4 particles were mainly coated by SiO_2. In comparison with MSN, the amount of Fe in MSN/AEM (6.26 wt%, Fig. 2b) and MSN/AEM–PTA (4.05 wt%, Fig. 2c) decreased, and the signals regarding to Cl and W were respectively observed in MSN/AEM and MSN/AEM–PTA. These results implied that AEM and PTA were respectively loaded on the surfaces of the corresponding composite nanoparticles. To verify this conclusion, the data from TGA and EDX were compared. The TGA spectra of MSN, MSN/AEM and MSN/AEM–PTA with 5% AEM were showed in Fig. 3. Based on the fact that the difference between the calcined residues of MSN (84.4 wt%) and MSN/AEM (75.3 wt%) is due to the presence of AEM, the amount of AEM and the corresponding content of Cl (1.01 wt%) in MSN/AEM could be estimated from the TG curves. This volume is near to the amount of 1.08 wt% which was got by detecting the surface of sample using EDX (Fig. 2b), implying that AEM were dominantly distributed on MSN/AEM surface. Similarly, the difference between the calcined residues of MSN/AEM (75.3 wt%) and MSN/AEM–PTA (80.0 wt%) was due to the presence of PTA. In consideration of the calcined residue of PTA is a mixture of WO_3 and P_2O_5 [19], the amount of PTA and W (15.2 wt%) in MSN/AEM–PTA could be estimated. And the amount of W on the surface of MSN/AEM–PTA was probed by EDX (Fig. 2c). This volume 14.4 wt% is near to 15.2 wt%, indicating that PTA anions were located on the surface of MSN/AEM–PTA. The characteristic peaks for C, O, Si, N and W in XPS spectrum shown in Fig. 4 further confirmed the composition of MSN/AEM–PTA.

3.1.2. FT-IR characterization

Fig. 5 showed the typical FT-IR spectra of MSN and MSN/AEM–PTA. Both 597 cm^{-1} and 467 cm^{-1} in MSN and MSN/AEM–PTA indicated that they contain both magnetite and maghemite [20]. The band at 1084 cm^{-1} attributed to the Si–O–Si stretching mode became stronger and broader for MSN/AEM–PTA, indicating that AEM was immobilized on SiO_2 through the condensation reaction [21]. The IR results above were according with XRD results (see Supplementary data Fig. S1). For MSN/AEM–PTA, the characteristic absorption bands at 2924.9 cm^{-1} and 2853.1 cm^{-1} were ascribed to CH_2 originated from silane coupling agent, suggesting the alkyl groups have been successfully grafted on MSN [22]. Moreover, the set of peaks at 978.7 cm^{-1}, 899.4 cm^{-1} and 821.3 cm^{-1} attributed to PTA presented in the spectrum of MSN/AEM–PTA demonstrating that the Keggin structure of PTA almost is remained [23]. The absorption peaks at 3400 cm^{-1} and 1628 cm^{-1} can be assigned to the adsorbed water on the silica shell or the silanol groups of the silica, which is a common characteristic of the silica formed in aqueous solutions [24].

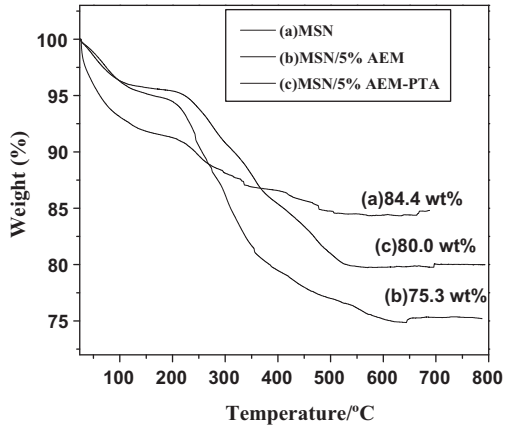

Fig. 3. The TGA spectra of MSN (a), MSN/AEM (b) and MSN/AEM–PTA (c) with 5% AEM.

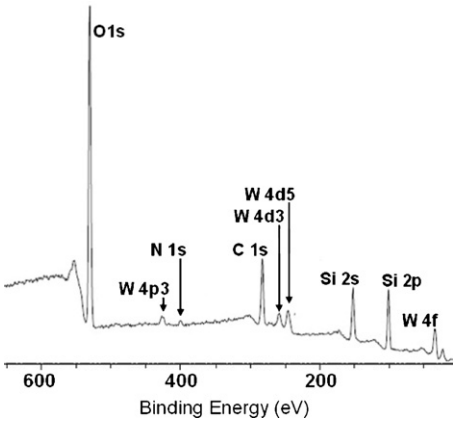

Fig. 4. The XPS spectrum of MSN/AEM–PTA with 5% AEM.

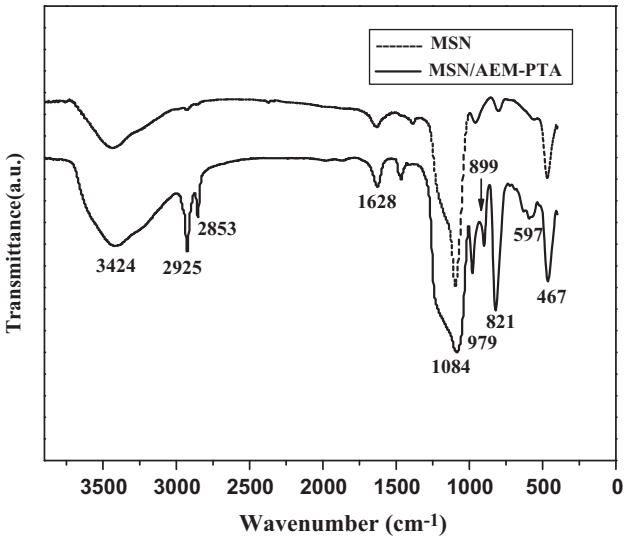

Fig. 5. The FT-IR spectra of MSN and MSN/AEM–PTA with 5% AEM.

3.1.3. Magnetic properties

The magnetic properties of MSN and MSN/AEM–PTA were measured by VSM. Field-dependence hysteresis loops of MSN and MSN/AEM–PTA were presented in Fig. 6. The saturation magnetization value of MSN was 18.18 emu/g at 300 K. The hysteresis and coercivity were almost undetectable, suggesting that MSN has superparamagnetic property at room temperature. The saturation magnetization value of MSN/AEM–PTA was 16.32 emu/g at 300 K, which was a little lower than that of MSN. The difference can be attributed to the nonmagnetic organic components which can reduce the total magnetization [25].

3.2. MSN/AEM–PTA used as catalytic microreactors in deep oxidative desulfurization

3.2.1. The oxidation of DBT to sulfone catalyzed by MSN/AEM–PTA nanoparticles

According to the characterization results, the structure of MSN/AEM–PTA particle was showed in Scheme 2. The as-prepared MSN/AEM–PTA particle has the core/shell structure. The core is magnetic SiO_2 to ensure the magnetic susceptibility of MSN/AEM–PTA, which makes the separation easy. The out layer is composed of the amphiphilic quaternary ammonium

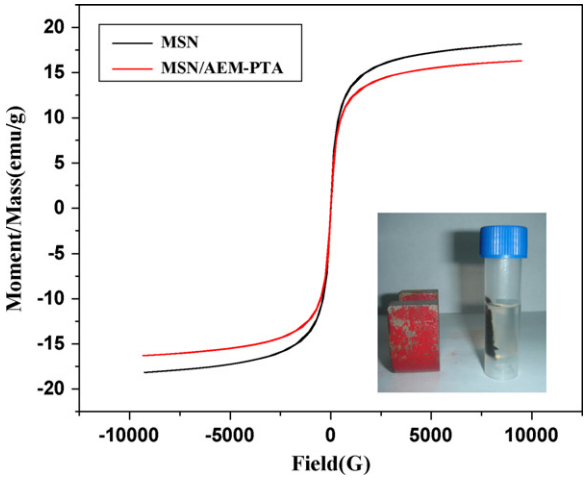

Fig. 6. The typical VSM magnetization curves of MSN and MSN/AEM–PTA.

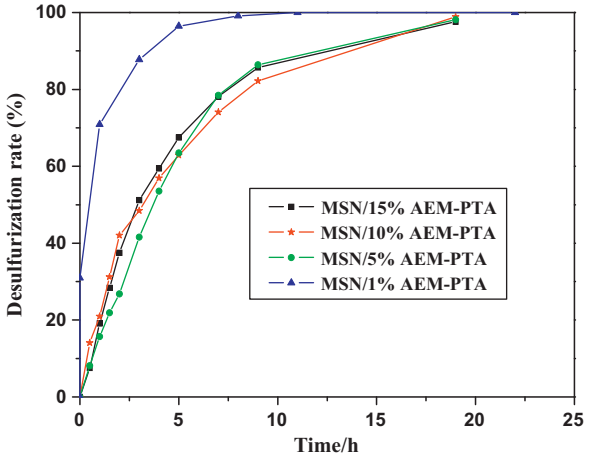

Fig. 7. The effect of the amount of AEM in MSN/AEM–PTA on the desulfurization rate. V(H_2O_2) = 300 μL; the amount of MSN/AEM–PTA = 0.12 g; DBT concentration = 2800 ppm.

heteropolyoxotungstate. It can be divided to hydrophilic area and hydrophobic area. The hydrophobic area formed by the alkyl chains of quaternary ammonium salt can introduce hydrophobic DBT to the surface of catalyst layer. The hydrophilic area formed by the moieties of heteropolyoxotungstate anion and quaternary ammonium cation plays the roles not only in the catalysis but also in storage of hydrophilic reactant (H_2O_2) and product (the sulfone). Based on the above structural features, it can be expected that MSN/AEM–PTA can play a good role in the catalysis and the simultaneous separation of catalyst and product. Namely, this material makes integration of micro-reactor and micro-extractor possible.

To investigate the influence of some reactive factors on desulfurization efficiency, the factors including the amount of AEM, the amount of H_2O_2, DBT concentration and recycling times of the catalyst were considered. The results were discussed in the following sections.

3.2.2. Influence of the amount of AEM on the desulfurization rate

Fig. 7 illustrated the effect of the amount of AEM in MSN/AEM–PTA on the deep oxidative desulfurization. The samples with AEM content ranging from 5% to 15% exhibited almost the same catalytic activity. They all took about 20 h to completely oxidize DBT. According to the detection limit of the method we used, DBT concentration in the end of reaction was less than 5 ppm (sulfur content less than 0.87 ppm). However, MSN/AEM–PTA with 1% AEM has an obvious superiority in the catalytic activity. The above results can be attributed to the following reason. Although the samples with the higher amount of AEM are favorable to the catalysis due to their higher amount of supported catalysts and their well dispersion in decahydronaphthalene, their high hydrophobicities are unfavorable to introduce reactant H_2O_2 into the hydrophilic inner layer of MSN/AEM–PTA. MSN/AEM–PTA with 1% AEM was amphiphilic and it can be wetted by both water and decahydronaphthalene (see Supplementary data Figs. S2 and S3). The results shown here indicate that the suitable amount of AEM immobilized onto the surface of MSN/AEM–PTA is very important in using MSN/AEM–PTA as diphase catalyst. Based on the results above mentioned, MSN/AEM–PTA with 1% AEM was selected in the following experiments.

3.2.3. Influence of the amount of H_2O_2 on the desulfurization rate

Fig. 8 showed the effect of the amount of H_2O_2 on the desulfurization rate. In the experiment, the different amounts of H_2O_2 (200 μL, 300 μL and 400 μL) were selected. As shown in Fig. 8, the amount of H_2O_2 has a strong influence on the reaction rate. When

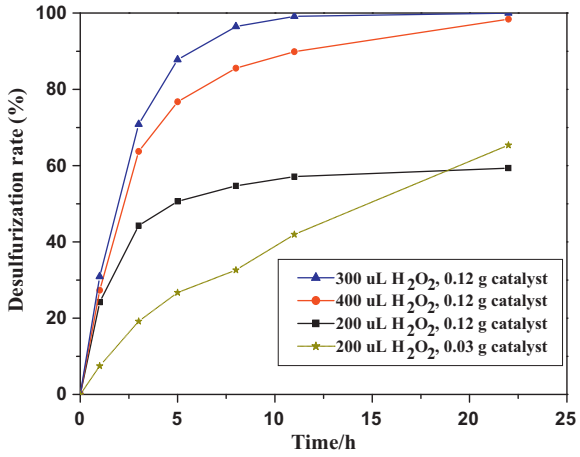

Fig. 8. The effect of the amount of H_2O_2 on the desulfurization rate. The amount of MSN/AEM–PTA with 1% AEM = 0.12 g; DBT concentration = 2800 ppm.

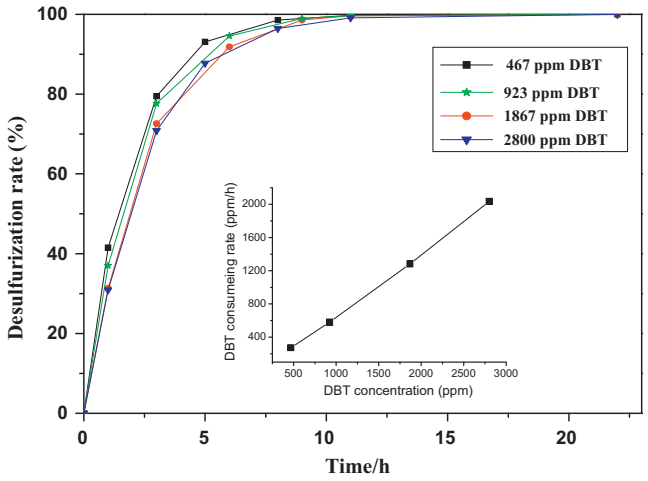

Fig. 9. The effect of DBT concentration on the desulfurization rate. The amount of MSN/AEM–PTA with 1% AEM = 0.12 g; $V(H_2O_2)$ = 300 μL.

the amount of H_2O_2 was increased from 200 μL to 400 μL, the DBT removal rate increased from 55% to 96% within 8 h. And the DBT removal rate could reach 100% for both 300 μL and 400 μL H_2O_2 within 22 h. It is worthy of note that DBT removal rate for 400 μL H_2O_2 is less than that for 300 μL. This finding is possibly related to the storage capability of the MSN/AEM–PTA nanoparticles for H_2O_2. Too much of H_2O_2 makes the surface of MSN/AEM–PTA nanoparticles hydrophilic, which is unfavorable to disperse the nanoparticles in hydrophobic medium due to the aggregation formed in this case. As a result, the reaction rate decreases.

Additionally, the molar ratio of 200 μL H_2O_2 to 0.0625 g DBT (5.8:1) far exceeds the stoichiometric requirement for complete oxidation of DBT to the corresponding sulfone. However, only 60% DBT was oxidized in case of using 200 μL H_2O_2. This finding implies that hydrogen peroxide was unexpectedly consumed in this situation. Barmatova et al. has found that iron could cause unproductive decomposition of H_2O_2 [26]. In fact, a few bubbles were observed when fresh catalyst nanoparticles were immersed in hydrogen peroxide. In the experiments, the catalytic reaction kept silence in presence of 0.12 g catalyst after 10 h reaction. The catalytic reaction was continued as the catalytic material was reduced (for example, 0.03 g of the catalytic material was used). The result further indicated that the contradiction between the experimental finding and theoretic conjecture is possibly related to a side reaction of MSN/AEM–PTA-catalyzed decomposition of H_2O_2. The results were shown in Fig. 8.

3.2.4. Influence of DBT concentration on the desulfurization rate

The effect of DBT concentration on the desulfurization rate was shown in Fig. 9. In the experiments, DBT concentration was selected from 467 to 2800 ppm. The amounts of H_2O_2 and MSN/AEM–PTA with 1% AEM were 300 μL and 0.12 g, respectively. Clearly, the desulfurization rate increased with the decrease of DBT concentration, indicating that the higher the initial concentration of DBT, the more difficult the complete removal of S [18]. The results shown in Fig. 9 also implied that it is potential to extend the range of DBT concentration in this case. Although the highest initial concentration of DBT in the present experiment was 2800 ppm, the active sites in the given amount of MSN/AEM–PTA nanoparticles were not yet fully saturated with DBT molecules. This conjecture can be verified by the relationship between initial concentration and initial reaction rate for DBT (shown in insert of Fig. 9). It was obviously showed that no rate saturation behavior was observed in the range of 467–2800 ppm. So, MSN/AEM–PTA nanoparticles may be used in the catalyzed desulfurization at the concentration range above 2800 ppm.

It is worth pointing out that MSN/AEM–PTA nanoparticles used as catalytic material have advantages in enhancement of reaction rate. For MSN/AEM–PTA, both catalytic moieties and reactant H_2O_2 are simultaneously concentrated in the limited region, which lead to high local concentrations of H_2O_2 and catalysts. Logically, this situation is especially important for the desulfurization with low concentration of DBT. Based on the results and discussion mentioned above, the structural MSN/AEM–PTA nanoparticles offer a logical strategy for the design of new catalysts used in water/organic diphase systems.

3.2.5. Recycling studies

The results of the recycling efficiency of MSN/AEM–PTA nanoparticles were shown in Fig. 10. The results obviously showed that MSN/AEM–PTA could be recycled effectively several times with satisfactory results. Interestingly, the performance of the fresh MSN/AEM–PTA is poorer than that of the reused one. Using reused particles, the desulfurization rate could rapidly exceed 90% in 3 h, reach about 100% in 5 h. This phenomenon observed may be attributed to the following reasons. The literature reported that H_2O_2 in the dried silica was less stable than that in the humid silica [27]. Firstly, the water molecules can stabilize hydrogen peroxide

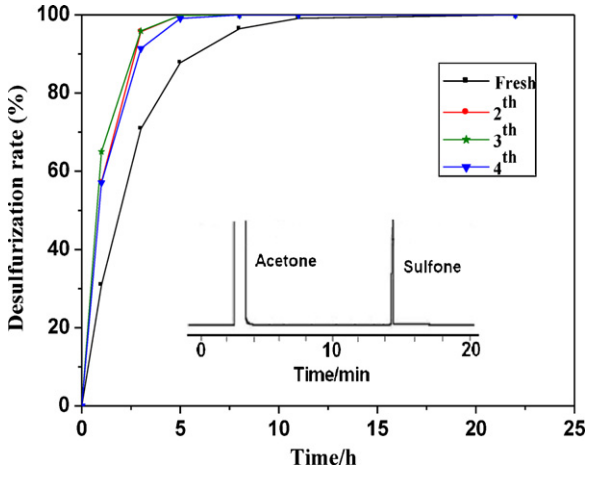

Fig. 10. The recycling efficiency of MSN/AEM–PTA used in the desulfurization. The inset displays the GC pattern of the acetone eluate of the used MSN/AEM–PTA.

through the formation an effective strengthening of hydrogen bonding to reduce hydrogen peroxide desorption rate from the silica matrix. Secondly, water molecules can neutralize catalytic sites of transition metals thus inhibiting chemical decomposition of the hydrogen peroxide. Additionally, hydrogen peroxide is often used to hydroxylate glass surface by increasing silanol groups [28]. Combining our finding and the aforementioned results in literature, the higher catalytic performance of the reused MSN/AEM–PTA is possibly related to the higher stability of H_2O_2 in reused catalytic material because there are more silanol groups in reused catalytic material to control the mobility of H_2O_2. Although the unexpected finding implies that the reused MSN/AEM–PTA nanoparticles have a good performance in the catalyzed desulfurization, to avoid the unproductive decomposition of H_2O_2 caused by the iron oxide in the prepared material should be highly regarded.

Furthermore, the recovered MSN/AEM–PTA nanoparticles were washed with acetone, and the sulfone was found in the acetone eluate (GC pattern as an insert shown in Fig. 10). The finding indicates that the sulfone could be extracted by MSN/AEM–PTA nanoparticles. Although the extraction ability of MSN/AEM–PTA nanoparticles is not perfect, the inspiration from this finding may be significant to design the multifunctional catalytic materials.

4. Conclusions

To get the reusable catalyst with easy separation and high catalytic performance used in the deep desulfurization using H_2O_2 as an oxidant, the composite nanospheres with superparamagnetism core and amphiphilic quaternary ammonium heteropolyoxotungstate shell were prepared. The results indicate that this protocol is feasible. The performances mentioned above are attributed to the specific structure and components of the prepared nanoparticles. The core with superparamagnetism makes separation of the nanoparticles easy under external magnetic field. The shell composed of the amphiphilic quaternary ammonium heteropolyoxotungstate could not only introduce hydrophobic DBT to the catalytic active sites with hydrophilicity but also store H_2O_2 and polar product in the hydrophilic layer. Additionally, the suitable amount of catalysts immobilized on the nanoparticles and hydrogen peroxide used as reactant are necessary for the high efficiency of desulfurization. The results here offer a new protocol that the micro-reactor and micro-extractor could be integrated by molecular design in one material. The inspiration from this protocol may be significant to design multifunctional catalytic materials used in the water/organic diphase systems.

Acknowledgments

The authors would like to thank the NSF of China (20576068, 20773084), SRF for ROCS, SEM, the Fundamental Research for the Central Universities (no. 2010ZYGX026), the NSF of Shaanxi Province (2005B12) and the donated funds of Chongben He financial support.

Appendix A. Supplementary data

Supplementary data associated with this article can be found, in the online version, at doi:10.1016/j.jhazmat.2011.11.063.

References

[1] US EPA, Regulatory announcement: heavy-duty engine and vehicle standards and highway diesel fuel sulfur control requirements, December 2000.
[2] F.F. Li, L.J. Song, L.H. Duan, X.Q. Li, Z.L. Sun, A frequency response study of thiophene adsorption in zeolite catalysts, Appl. Surf. Sci. 253 (2007) 8802–8809.
[3] F.M. Collins, A.R. Lucy, C. Sharp, Oxidative desulphurisation of oils via hydrogen peroxide and heteropolyanion catalysis, J. Mol. Catal. A: Chem. 117 (1997) 397–403.
[4] K. Yazu, Y. Yamamoto, T. Furuya, K. Miki, K. Ukegawa, Oxidation of dibenzothiophenes in an organic biphasic system and its application to oxidative desulfurization of light oil, Energy Fuel 15 (2001) 1535–1536.
[5] A. Srivastav, V.C. Srivastava, Adsorptive desulfurization by activated alumina, J. Hazard. Mater. 170 (2009) 1133–1140.
[6] X. Ma, L. Sun, C. Song, A new approach to deep desulfurization of gasoline, diesel and jet fuel by selective adsorption for ultra-clean fuels and for fuel cell applications, Catal. Today 77 (2002) 107–116.
[7] C.P. Huang, B.H. Chen, J. Zhang, Z.C. Liu, Y.X. Li, Desulfurization of gasoline by extraction with new ionic liquids, Energy Fuel 18 (2004) 1862–1864.
[8] B. Wang, J.P. Zhu, H.Z. Ma, Desulfurization from thiophene by SO_4^{2-}/ZrO_2 catalytic oxidation at room temperature and atmospheric pressure, J. Hazard. Mater. 164 (2009) 256–264.
[9] J.M. Campos-Martin, M.C. Capel-Sanchez, P. Perez-Preas, J.L.G. Fierro, Oxidative processes of desulfurization of liquid fuels, J. Chem. Technol. Biotechnol. 7 (2010) 879–890.
[10] W.S. Zhu, H.M. Li, X. Jiang, Y.S. Yan, J.D. Lu, L.N. He, J.X. Xia, Commercially available molybdic compound-catalyzed ultra-deep desulfurization of fuels in ionic liquids, Green Chem. 10 (2008) 641–646.
[11] A. Nisar, J. Zhuang, X. Wang, Construction of amphiphilic polyoxometalate meostructures as a highly efficient desulfurization catalyst, Adv. Mater. 23 (2011) 1130–1135.
[12] D.J. Monticello, Biodesulfurization and the upgrading of petroleum distillates, Curr. Opin. Biotechnol. 11 (2000) 540–546.
[13] B.H. Kim, H.Y. Kim, T.S. Kim, D.H. Park, Selectivity of desulfurization activity of desulfovibrio desulfuricans M6 on different petroleum products, Fuel Process. Technol. 43 (1995) 87–94.
[14] C. Li, Z.X. Jiang, J.B. Gao, Y.X. Yang, S.J. Wang, F.P. Tian, F.X. Sun, X.P. Sun, P.L. Ying, C.R. Han, Ultra-deep desulfurization of diesel: oxidation with a recoverable catalyst assembled in emulsion, Chem. Eur. J. 10 (2004) 2277–2280.
[15] H. Li, P. Zhang, L. Zhang, T. Zhou, D.D. Hu, Composite microspheres with PAM microgel core and polymerisable surfactant/polyoxometalate complexes shell, J. Mater. Chem. 19 (2009) 4575–4586.
[16] S.F. Song, S.K. Shen, X.A. Cui, D.D. Yao, D.D. Hu, Microhydrogel surface-supported quaternary ammonium peroxotungstophosphate as reusable catalytic materials for oxidation of DBT, React. Funct. Polym. 71 (2011) 512–519.
[17] S.C. Tsang, C.H. Yu, X. Gao, K. Tam, Silica-encapsulated nanomagnetic particle as a new recoverable biocatalyst carrier, J. Phys. Chem. B 110 (2006) 16914–16922.
[18] G.F. Zhang, F.L. Yu, R. Wang, Research advances in oxidative desulfurization technologies for the production of low sulfur fuel oils, Petrol. Coal 51 (2009) 196–207.
[19] J.D. Kim, I. Honma, Highly proton conducting hybrid materials synthesized from 12-phosphotungstic and hexadecyltrimethylammonium salt, Solid State Ionics 176 (2005) 547–552.
[20] H. Wang, Q.W. Chen, L.X. Sun, H.P. Qi, X. Yang, S. Zhou, J. Xiong, Magnetic-field-induced formation of one-dimensional magnetite nanochains, Langmuir 25 (2009) 7135–7139.
[21] Y.S. Li, P.B. Wright, R. Puritt, T. Tran, Vibrational spectroscopic studies of vinyltriethoxysilane sol–gel and its coating, Spectrochim. Acta Part A 60 (2004) 2759–2766.
[22] Y.F. Shaa, C.H. Dengb, B.Z. Liua, Development of C18-functionalized magnetic silica nanoparticles as sample preparation technique for the determination of ergosterol in cigarettes by microwave-assisted derivatization and gas chromatography/mass spectrometry, J. Chromatogr. A 1198–1199 (2008) 27–33.
[23] C. Rocchiccioli-Deltcheff, M. Fournier, R. Franck, R. Thouvenot, Vibrational investigations of polyoxometalates. 2. Evidence for anion–anion interactions in molybdenum(VI) and tungsten(VI) compounds related to the Keggin structure, Inorg. Chem. 22 (1983) 207–216.
[24] X.B. Zhao, X.Y. Liu, C.X. Ding, Acid-induced bioactive titania surface, J. Biomed. Mater. Res. 75A (2005) 888–894.
[25] K.V. Shafi, A. Ulman, A. Dyal, X. Yan, N.L. Yang, C. Estournes, L. Fournes, A.Wattiaux, H. White, M. Rafailovich, Magnetic enhancement of γ-Fe_2O_3 nanoparticles by sonochemical coating, Chem. Mater. 14 (2002) 1778–1787.
[26] M.V. Barmatova, I.D. Ivanchikova, O.A. Kholdeeva, A.N. Shmakov, V.I. Zaikovskii, M.S. Melgunov, Magnetically separable titanium–silicate mesoporous materials with core–shell morphology: synthesis characterization and catalytic properties, J. Mater. Chem. 19 (2009) 7332–7339.
[27] J. Zegliński, A. Cabaj, M. Strankowski, J. Czerniak, J.T. Haponiuk, Silica xerogel–hydrogen peroxide composites: their morphology, stability, and antimicrobial activity, Colloids Surf. B: Biointerfaces 54 (2007) 165–172.
[28] K.J. Seu, A.P. Pandey, F. Haque, E.A. Proctor, Effect of surface treatment on diffusion and domain formation in supported lipid bilayers, Biophys. J. 92 (2007) 2445–2450.